

Back-Projection Cortical Potential Imaging: Theory and Results

Dror Haor,* Reuven Shavit, Moshe Shapiro, and Amir B. Geva

Abstract—Electroencephalography (EEG) is the single brain monitoring technique that is non-invasive, portable, passive, exhibits high-temporal resolution, and gives a direct measurement of the scalp electrical potential. A major disadvantage of the EEG is its low-spatial resolution, which is the result of the low-conductive skull that “smears” the currents coming from within the brain. Recording brain activity with both high temporal and spatial resolution is crucial for the localization of confined brain activations and the study of brain mechanism functionality, which is then followed by diagnosis of brain-related diseases. In this paper, a new cortical potential imaging (CPI) method is presented. The new method gives an estimation of the electrical activity on the cortex surface and thus removes the “smearing effect” caused by the skull. The scalp potentials are back-projected CPI (BP-CPI) onto the cortex surface by building a well-posed problem to the Laplace equation that is solved by means of the finite elements method on a realistic head model. A unique solution to the CPI problem is obtained by introducing a cortical normal current estimation technique. The technique is based on the same mechanism used in the well-known surface Laplacian calculation, followed by a scalp-cortex back-projection routine. The BP-CPI passed four stages of validation, including validation on spherical and realistic head models, probabilistic analysis (Monte Carlo simulation), and noise sensitivity tests. In addition, the BP-CPI was compared with the minimum norm estimate CPI approach and found superior for multi-source cortical potential distributions with very good estimation results ($CC > 0.97$) on a realistic head model in the regions of interest, for two representative cases. The BP-CPI can be easily incorporated in different monitoring tools and help researchers by maintaining an accurate estimation for the cortical potential of ongoing or event-related potentials in order to have better neurological inferences from the EEG.

Index Terms—Cortical potential imaging, back-projection, surface Laplacian, finite element method, head modeling.

Manuscript received February 5, 2017; revised February 27, 2017; accepted February 28, 2017. Date of publication March 9, 2017; date of current version June 29, 2017. This work was supported in part by EIMindA Ltd., and in part by grants from the Israeli OCS through the MAGNET Program. *Asterisk indicates corresponding author.*

*D. Haor is with the Department of Electrical and Computer Engineering, Ben-Gurion University of the Negev, Beer-Sheva 653256, Israel, and also with EIMindA, Ltd., Herzliya 4673314, Israel.

R. Shavit and M. Shapiro are with the Department of Electrical and Computer Engineering, Ben-Gurion University of the Negev, Beer-Sheva 653256, Israel.

A. B. Geva is with the Department of Electrical and Computer Engineering, Ben-Gurion University of the Negev, Beer-Sheva 653256, Israel, and also with EIMindA, Ltd., Herzliya 4673314, Israel.

Digital Object Identifier 10.1109/TMI.2017.2679756

I. INTRODUCTION

ELECTRICAL brain activity is spatially distributed within the head structure and evolves with time. Nowadays, several modalities of functional brain imaging are available, including PET, SPECT, fMRI, MEG, and EEG. Apart from EEG, most of these modalities are very expensive, non-portable, ionizing, or maintain non-direct measurement of the brain electrical activity. Although high spatial resolution is mostly feasible with these modalities, low temporal resolution of the brain activity is a huge drawback, preventing researchers from capturing generation of those split-second seizures or cognitive bio-markers. Another aspect that is often overlooked is the imaging modality competence to integrate into monitoring and stimulation tools. The need for such a brain imaging modality, which can operate under different types of electric or magnetic stimulation while simultaneously monitoring the brain activity, comes from the recently developed approach that brain-related diseases should be treated with an adaptive treatment that changes according to the presently acquired monitoring results. EEG is the single brain monitoring technique that is non-invasive, portable, passive, and gives a direct measurement of the electrical potential signals on the scalp. These advantages join to provide high temporal resolution sampled by a simple sensor, which together makes it the most widely used brain monitoring technique. The main drawback of the EEG for scalp measurement is its poor spatial resolution. The physical mechanism that degrades the spatial resolution of EEG can be related to the poor conductivity of the skull layer [1]–[3]. This has the effect of “blurring” the currents (and potentials) coming from within the brain.

In the last two decades, tremendous effort has been made to enhance the spatial resolution of the conventional EEG, mainly using three classes of methods [4], [5]. The first class of methods is *source localization*, i.e., trying to find the location, orientation, and amplitude of the different brain sources that generate scalp potentials that best fit the scalp measured EEG. Due to the “blurring” effect caused by the electrical properties of the skull layer and the finite number of EEG electrodes on the subject’s scalp, the source localization solution is not unique without any a priori information [4], [6]. The second class of high-resolution EEG imaging is the *current estimation* methods [1]–[3] that are based on two-dimensional image sharpening procedures that operate on the potentials measured on the scalp surface, mostly known as

the scalp current density (SCD) or the surface Laplacian (SL), which can be used to estimate the normal currents flowing from the skull into the scalp tissue. These procedures make use of the unique nature of the scalp's normal currents reaching the outer scalp-air interface and must transform them into tangential currents. The major drawback of most of these methods is that they do not take into account the head's physical geometry and the tissue's electrical properties, which hold much of the information about the "blurring" effect. Babiloni *et al.* [3] developed a realistic Laplacian technique that takes into account the skull thickness, but still lacks the true effect of the skull conductivity in his model. The third class of methods is *cortical potential imaging* (CPI). CPI is a general title for methods that seek to estimate the potential distribution on the cortical surface using only the scalp potentials measured by EEG electrodes. These methods can be divided into two major types: The first, and the most used type of CPI methods, are the regularization-optimization methods. This type includes the generalized singular value decompositions (SVD) method and its variants [7], the weighted inverse method [8], which is a generalization of the well-known special case of LERETA algorithm [9]. In addition, the constrained inverse method [10] enables the introduction of some constraints to the solution. [11], [12]. Another similar solution is the minimum-norm (MN) estimation [12]–[17], which tries to find a solution having minimum energy that best corresponds with the measured EEG data. All of these methods try to find the cortical potentials that best agree with a combination of constraints on the whole solution. This type of constraint can be the minimum energy of the solution, smoothness, region of interest, and more. In general this is done by minimizing the functional in Eq. (1)

$$F(u_c) = \|Au_c - u_s\|^2 + \lambda L(u_c) \quad (1)$$

where u_c and u_s are the cortical and scalp potentials, A is the lead field matrix that connects the scalp to the cortical potentials. $L(u_c)$ is selected according to the chosen minimization scheme (e.g., $L(u_c) = \|u_c\|^2$ for minimization of energy), and $\|\cdot\|$ is the L^2 norm. The first term of the objective function is the error term formalized in the least squares sense. The second term is the regularization term, which helps solve this ill-posed minimization problem by using the regularization factor λ that can be selected using various methods [18]–[20]. All of these methods are driven by the scalp potentials and are not constant for a unique head model. This can be problematic for measurements of a massive number of subjects over many time-points, and requires calculation of a different parameter set for each scalp potential at each time-point. The second type of CPI method is the forward-iterative method [21]–[23], which is based on solving the Laplace equation (LE) in the bounded volume between the cortex and the scalp while defining cortical potential distribution as the excitation (i.e., the forward problem). The iterative method solves the forward problem for an initial cortical potential distribution and performs a multi-dimensional optimization scheme in order to converge to the correct potential distribution. These methods are typically computationally exhaustive and very sensitive to the local minima problem and the initial

solution, and thus will not always give the correct potential distribution.

Although some of the above mentioned CPI methods can give good results, to date they have not shown robustness and consistency along a large number of subjects and cortical potential solutions. They also did not show full sensitivity analysis comparing the proposed solution with simulated "true" cortical potentials, except for some specific results.

In this work, a new cortical potential imaging method is presented. The scalp potential distribution is back-projected (BP-CPI) to the cortex surface using an electroquasistatic (EQS) mechanism. Using the conductivity information of the realistic head model maintained by a single subject MRI T1 scan, along with scalp potentials measured using EEG electrodes, we introduce a novel cortical current estimation technique. The estimated normally-oriented cortical current is used to generate a solution to LE inside the volume above the cortical surface and below the scalp. According to [24], if LE is solved in a volume wrapped by known boundary conditions, the solution will be single-valued and unique. The algorithm makes use of the finite element method (FEM) to solve the LE in order to account for tissues with non-homogeneous conductivity properties. The BP-CPI estimates the cortical currents by employing the same mechanism used in the SL calculation with a back-projection technique to maintain an accurate estimation on the cortical surface.

The novelty and merit of the proposed algorithm, compared to existing CPI techniques, is three-fold: 1) introduction of a second BC, transforms the problem from a non-unique, ill-posed inverse problem into a forward-problem-variant, known to have a single, stable, and unique solution; 2) the solution to the BP-CPI problem is reduced into a simple matrix inversion problem, which gives a fast solution in only one iteration of calculation, avoiding the need for a computation exhaustive technique; and 3) using a novel back-projection mechanism, which exploits the realistic head model conductivities, the technique obtains highly accurate cortical potentials estimation.

This paper is organized as follows: section II gives a full description of the method and the head modeling used, in addition to a description of the forward solution used for the BP-CPI validation, which was done by the Sim4Life commercial electromagnetic (EM) simulation software. Section III presents simulative results on spherical and realistic head models, comparison between the BP-CPI to the minimum norm (MN) CPI method, results of a Monte Carlo simulation and an investigation of the effect of noise on the BP-CPI estimation. Finally, section IV concludes this study.

II. MATERIALS AND METHODS

A. The Back-Projection Solution

The volume conductor problem can be formulated in terms of a quasistatic Poisson equation. If we select a volume with no sources, the Poisson equation reduces to LE, which can be solved with a unique solution if and only if the boundary condition (BC) on the volume boundaries are known [24].

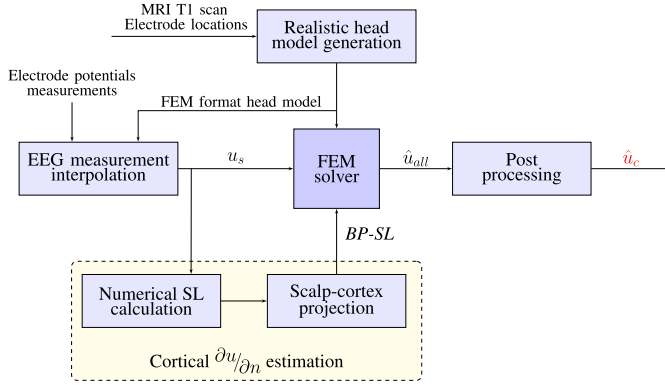


Fig. 1. BP-CPI algorithm block diagram.

When dealing with the volume between the scalp and cortex surfaces, here denoted as the solution volume, we can confidently assume that no sources exist due to the fact that no neural cells lie in that region.

Let the domain V denote the solution volume, bounded by the scalp and cortex surfaces Ω_s and Ω_c , respectively. Solving LE for the potentials $u(r)$ in V wrapped by a constrained BC will give the back-projection (BP) cortical solution, or *BP-CPI*. The BP-CPI solution makes use of an estimated cortical BC to wrap the solution volume. By doing so, the problem alters from a classic inverse-problem to a variation of a forward-problem which is known to have a unique solution. The LE formulation can be written in the form:

$$\nabla \cdot (\sigma \nabla u) = 0 \quad r \in V \quad (2)$$

The BCs on the scalp are:

$$\frac{\partial u}{\partial n} = 0 \quad r \in \Omega_s \quad (3)$$

$$u = u_s \quad r \in \Omega_s \quad (4)$$

where u_s is the interpolated potential distribution acquired from the measured EEG electrodes, $\sigma(r)$ is the inhomogeneous conductivity in V , and (3) illustrates the fact that no normal current exits the scalp surface. The estimated BC on the cortex is,

$$\frac{\partial u}{\partial n} = BP-SL \quad r \in \Omega_c \quad (5)$$

in which the back-projected surface Laplacian (*BP-SL*) is the estimated normal potential derivative on the cortex. The BP-CPI algorithm block-diagram is presented in Fig. 1. EEG electrodes' positions, in addition to a single T1 MRI scan, are used to generate a meshed FEM-based head model which includes the electrode positions on the scalp. Then, electrode potentials are interpolated over the entire scalp surface mesh nodes in order to obtain the scalp potentials u_s to be used as BC and solve the LE by the FEM solver. The selected interpolation method is the "thin plate" spline interpolation method [25], which was found to give the best results when compared with the actual scalp potentials, and, in general, is computationally faster than other spline interpolation schemes. u_s is also used to find the estimated cortical BC *BP-SL*.

The estimation is done in two stages: 1) SL calculation evaluated on the scalp surface, and 2) back-projection of the scalp SL onto the cortical surface to serve as the second BC for the FEM solver. The FEM solver finds the unique solution \hat{u}_{all} for the LE constrained by the two BCs within the entire solution volume. In the final stage, a simple post-processing stage extracts the desired estimated cortical potentials \hat{u}_c .

In this work we introduce a physics-based BC on the cortical surface in order to give a full description of the back-projection problem and maintain a single and unique solution for the potentials in the entire solution volume. Furthermore, by solving the LE using the described scheme, we capture the cortical potentials due to both the normal and tangential potential derivatives.

B. Cortical Current Estimation

Much of the ability to perform a correct scalp-to-cortex back-projection is based on the knowledge of an accurate potential normal derivative as shown in Eq. (5). In order to estimate the cortical current correctly we make use of the surface Laplacian (SL) operator calculated based on measured scalp potentials, as described in Eq. (6)

$$\begin{aligned} \nabla_{sd} \cdot J_s &= \nabla_{sd} \cdot \sigma_s \nabla_{sg} u_s = \sigma_s \underbrace{\nabla_s^2 u_s}_{SL} \\ I_{in} &= \int_c J_t dl = \int_s \nabla_{sd} \cdot J_s dS \\ &= \sigma_s \int_s SL \cdot dS = \sigma_s \cdot SL \cdot \Delta S \end{aligned} \quad (6)$$

where the scalp is composed from finite element cells with scalp-area of ΔS , conductivity of σ_s , and potential of u_s . I_{in} is the total normal current entering the element (with density J_s), J_t is the tangential current exiting it, and ∇_{sg} and ∇_{sd} are the surface gradient and surface divergence operators, respectively.

Numerical Surface Laplacian: The SL operator estimates the normal currents flowing from the skull to the scalp layer by using the fact that any normal current reaching the scalp outer surface vanishes due to the BC described in Eq. (3) and must transform to the tangential direction. The BP-CPI implements Le *et al.*'s [26] method for the SL estimation, which was found to be a robust and fast method. The method estimates the SL values through a local planar parametric space using Taylor expansion around each electrode site, with the least-squares technique. In addition, we implemented spatial low-pass filters pre- and post-calculation adapted to our head models optimized to cancel high frequency noises that can cause instability in the SL calculations. It should be noted that this procedure calculates the SL on the scalp surface.

Scalp-Cortex Projection: For the purpose of imposing cortical current as BC, the SL, which estimates the skull normal currents calculated on the scalp surface, must be projected from the scalp surface onto the cortex. Okamoto and Dan *et al.* [27] developed an algorithm for the transcranial projection of head-surface points onto the cortical surface of structural images. The algorithm takes into consideration the exact meshing of the scalp and cortex surfaces and finds the best

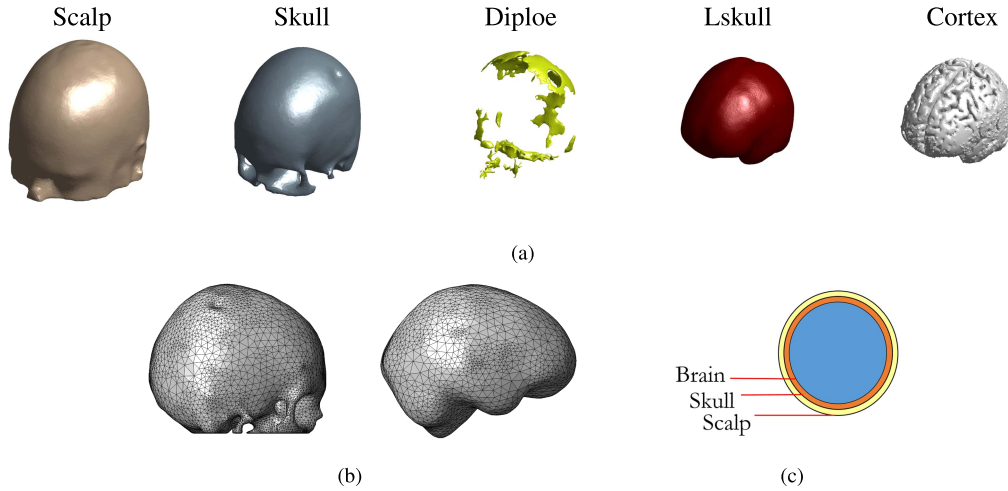


Fig. 2. Head modeling and meshing. (a) different layers extracted by the realistic head modeling algorithm, from left to right: scalp, skull, diploe, Lskull, cortex; (b) meshing example of skull (left) and Lskull (right) surfaces; (c) three-layer spherical head model.

fitting scalp vertex that corresponds to its source on the cortex. This method is used as a part of the BP-CPI algorithm to project the scalp SL on the cortical surface to perform as a normal potential derivative estimation.

Once we calculate the SL on the scalp surface and its projection on the cortical surface, the SL result should take the form of current density, including a projection factor (PF) with units of $[m^2/ohm]$. The definition of the PF is as noted in Eq. (7)

$$PF = \frac{J_{cortex}}{SL} \quad (7)$$

It can be shown [1], [28] that:

$$J_{cortex} \approx J_k \approx J_s = (-\sigma_s d_s) SL \quad (8)$$

where d_s is the local scalp thickness. The current entering the scalp can be approximated by the normal current density J_k flowing from the skull into the scalp tissue. The cortex currents J_{cortex} can be considered as a good approximation to J_k while assuming a high resistive skull layer. Substitution of (8) into (7) yields,

$$PF = -\sigma_s d_s \quad (9)$$

A few general assumptions are made in the usage of the SL and PF: 1) Head tissues are very thin relative to the electric field curvature, which is certainly true due to the very low frequency of the electric field and the dimensions of the head tissues and layer, which are a few millimeters each. 2) Most of the current coming from within the brain is directed normal to both the cortical and skull surfaces, which is mostly true due to low conductivity of the skull layer, which almost completely reduces the spreading of currents, and the internal structure below the cortex surface that enables mostly normal currents to flow. This assumption enables back-projection of the SL onto the cortical surface. This claim was tested in Sec. III-A, and was found valid for both spherical and realistic head models.

C. Head Modeling and Electrodes Alignment

Van Uitert *et al.* [29] have shown that realistic head modeling is crucial for acquiring a high-resolution CPI. An automatic segmentation and meshing algorithm was developed for the purpose of rapid single-subject realistic head model generation. The algorithm uses, among other meshing and image processing developed tools, the statistical parametric mapping (SPM) package [30], brain extraction tool (BET) software [31], and iso2mesh toolbox [32]. The result is a tetrahedral head mesh, partitioned into different sub-divisions for various bone and tissues as depicted in Figs. 2(a) and 2(b).

Each layer receives a homogeneous isotropic conductivity value. The realistic head model used in this work includes the following layers: scalp, higher skull (compact bone), intermediate skull (Diploe), and the inner/lower skull, or “Lskull” (compact bone) with conductivities of 0.33, 0.0042, 0.0286, and 0.0042 [S/m], respectively, and was found to be a good representation for these layers’ properties [33]–[36]. In addition, this head model takes into account air cavities sparsely located within the head. The cerebral spinal fluid (CSF) and cortical surfaces are not included in the model. The estimation will only be projected to the lower skull (Lskull) surface, which will be referred to as the cortical surface with cortical potentials. We do not expect any major changes in the potential distribution between the Lskull and the cortex surface because of the relatively high conductivity values in the volume below the Lskull surface.

The realistic head modeling (RHM) algorithm uses highly detailed T1 weighted MRI scans of a single subject with an in-plane resolution of 0.67 mm by 0.67 mm and slice thickness of 1 mm (3-D MP-RAGE, TR = 2000 ms, TE = 2.99 ms, 8° flip). The MRI scans were aligned and normalized according to the Montreal Neurological Institute (MNI) template ICBM152 [37], for future co-registration and comparison between subjects.

With the aim of validating our BP-CPI algorithm, we also generated a simplified three-layer spherical head model (SHM) as shown in Fig. 2(c). The spherical head model has three

TABLE I
HEAD MODELS MESH INFORMATION

| Model | E | MEV | N_c | N_s | N |
|-------|------|-------|-------|-------|-----|
| RHM | 499K | 4.38 | 3K | 6K | 82K |
| SHM | 300K | 2.9 | 2.5K | 2.5K | 53K |



Fig. 3. EEG electrodes alignment to scalp surface. Three views of the scalp surface reconstructed from the subject's MRI are shown with small disks on the surface of the scalp representing electrode positions after alignment.

spherical layers with radii of 8, 8.5, and 9 cm and conductivity values of 1, 0.0125, and 1 S/m for the cortex, skull, and scalp layers, respectively. Complete information of the realistic and spherical head models mesh is presented in Table I, where E , N_c , N_s , N , and MEV represent the total number of elements, number of cortex nodes, number of scalp nodes, total number of nodes, and mean element volume [mm^3], respectively.

The HydroCel Geodesic EEG sensor net (Electrical Geodesic Inc.) with 128 electrodes, denoted here as EGI128, was used as the high resolution EEG system. The EGI128 has an inter-electrode spacing of about 2.5 cm. Slutzky *et al.* [38] concluded that for high-resolution EEG, electrode spacing of 2 cm or less is needed. Although the EGI128 sampling density is still insufficient to resolve the topography of any cortical source from the scalp, it likely provides an adequate representation of the scalp topography of most brain electrical events of interest to researchers and clinical practitioners.

EEG electrodes' locations used in the electrodes alignment procedure originated in the general MNI coordinates given by the manufacturer. In order to align the system to the subjects' scalp surface we used a simple optimization scheme that used linear translation to find the best fit between the subject's scalp to the electrodes' locations. Finally, a single node on the scalp mesh is selected for each electrode by finding the closest scalp node to the radial projection of the electrode to the cortex surface. Results of the described alignment procedure are shown in Fig. 3. Note that the head model presented here is trimmed at the height of the nose and the lower part of the ear. Due to this, only 124 electrodes of the EGI128 were registered for this electrode system. Unregistered electrodes are placed very low on the face and neck and thus would not have added information to the BP-CPI estimation.

D. FEM Formulation

The FEM formulation for the BP-CPI algorithm will be briefly described here and found in more detail in [39]. The variational principle for the LE gives the functional $F(u)$,

which is given in Eq. (10)

$$F(u) = \frac{1}{2} \iiint_V [-\nabla \cdot (\sigma \nabla u)] \cdot u^* \cdot dv \quad (10)$$

Using Green's theorem we can rewrite Eq. (11) in the form,

$$F(\varphi) = \frac{1}{2} \iiint_V \sigma |\nabla u|^2 \cdot dv - \frac{1}{2} \iint_{\Omega_s + \Omega_c} \sigma u \frac{\partial u}{\partial n} ds \quad (11)$$

The surface integral is fully defined by applying Eq. (3) and (6), and the FEM formulation will result in a global matrix equation:

$$\left[\underline{\underline{A}}_g \right] \cdot \left[\underline{\underline{u}}_g \right] = \left[\underline{\underline{b}}_g \right] \quad (12)$$

where $\left[\underline{\underline{A}}_g \right]$ represents the connections between volume nodes, $\left[\underline{\underline{u}}_g \right]$ are the unknown potentials within the solution volume, and $\left[\underline{\underline{b}}_g \right]$ represent the connections between surface nodes, imposing our estimation of the cortical normal potential derivative BC ($\partial u / \partial n$) and the termination scalp BC ($\partial u / \partial n = 0$). Next, two internal BCs are imposed on our solution through linear constraints (LC) on (12) [40]. The first is expressed in Eq. (5) and the second is the imposition of a continual normal current on every surface S_i separating two different tissues with conductivities σ_{1i} and σ_{2i} , as shown in Eq. (13):

$$\left[\sigma_{2i} \nabla u_j^+ - \sigma_{1i} \nabla u_j^- \right] \cdot \hat{n} \Big|_{S_i} = 0 \quad (13)$$

which yields a linear relation between the potential of each surface node u_j and its surrounding nodes u_j^+ and u_j^- directly above and below, in the normal direction \hat{n} and in distances of Δn_j^+ and Δn_j^- , respectively, as shown in Eq. (14)

$$u_j = \zeta_{S_i j} \cdot u_j^- + (1 - \zeta_{S_i j}) \cdot u_j^+ \quad (14)$$

$$\zeta_{S_i j} = \frac{1}{1 + \chi_{S_i} \cdot (\Delta n_j^- / \Delta n_j^+)}$$

where χ_{S_i} is the conductivity ratio between the two elements' conductivity above and below node j of surface S_i . This type of formulation is dependent on the meshing grid and in general may not always be applicable.

Both internal BCs are enforced through evaluating the vector $\left[\underline{\underline{c}} \right]$ and matrix $\left[\underline{\underline{P}} \right]$ that imposes LC on the solution $\left[\underline{\underline{A}}_g \right]$ to generate an updated global matrix equation (15). Vector $\left[\underline{\underline{c}} \right]$ imposes direct scalp potential values (Dirichlet's BC) and $\left[\underline{\underline{P}} \right]$ is a matrix dictating the linear dependences as shown in Eq. (14), to impose normal current continuity BC.

$$\left[\underline{\underline{A}}'_g \right] \cdot \left[\underline{\underline{u}}_g \right] = \left[\underline{\underline{b}}'_g \right] \quad (15)$$

where:

$$\left[\underline{\underline{A}}'_g \right] = \left[\underline{\underline{P}} \right]^T \cdot \left[\underline{\underline{A}}_g \right] \cdot \left[\underline{\underline{P}} \right] \quad (16)$$

$$\left[\underline{\underline{b}}'_g \right] = \left[\underline{\underline{P}} \right]^T \cdot \left(\left[\underline{\underline{b}}_g \right] - \left[\underline{\underline{A}}_g \right] \cdot \left[\underline{\underline{c}} \right] \right) \quad (17)$$

E. Validation by Forward Solution

An accurate, stable, and independent forward solution to the volume conductor problem in a realistic head was implemented as a part of this research. The solution is based on Sim4Life 1.2 software (by ZMT) [41]. Its numerical algorithm is based on FEM. The simulation performed with Sim4Life in this research only involves forward solution with the single purpose of generating a “true solution” to compare with the BP-CPI results. Different sources’ (electrical dipoles) distributions are placed inside the cortex volume, the sources’ strength and orientation were selected, and the forward FEM solution was obtained with these sources’ excitations. Next, the scalp and cortical potentials were extracted from the solution. Scalp “true potentials” were used as the input to the BP-CPI algorithm and its output, the estimated cortical potentials, was compared to the cortex “true potentials”.

The analytical solution using harmonics spherical modes of the potential distribution for the case of a dipole placed inside the cortex volume for the spherical head model is well-known [1], and therefore this case was implemented. The analytical potential distribution using spherical harmonics on the scalp and cortex surfaces was calculated for the case of nine normally oriented dipole structure, formed in L-shape, inside a spherical head model. This source distribution was selected as a deductive case on a spherical head model due to the proximity of the sources (about 2 cm) and their unique spatial position. In addition, this distribution tests both horizontally and vertically aligned cortical sources, which may be present in *in vivo* cases involving motor or auditory tasks [42], [43]. The exact same source distribution was simulated using Sim4Life for validation. Comparison of the results is shown in Fig. 4. It is seen that the Sim4Life and the analytical solution are in very good agreement.

Error Quantitative Evaluation: Here, and in the rest of the paper, we use Pearson’s correlation coefficient (CC) and the relative error (RE) as measures to quantify similarity. The CC and RE definitions are presented in Eqs. (18) and (19)

$$CC = \frac{\sum_{i=1}^N (u_i^A - \bar{u}^A) (u_i^B - \bar{u}^B)}{\sqrt{\sum_{i=1}^N (u_i^A - \bar{u}^A)^2} \sqrt{\sum_{i=1}^N (u_i^B - \bar{u}^B)^2}} \quad (18)$$

$$RE = \frac{1}{N} \sum_{i=1}^N \left| \frac{u_i^A - u_i^B}{u_i^B} \right| \quad (19)$$

where u_i^A and u_i^B are the potential values at the i^{th} node of potential distributions A and B, respectively. The bar sign represents the mean of the vector, N is the total number of nodes for the potential distributions, and i runs over all nodes $i = 1 \dots N$

III. RESULTS

This section is divided into four parts: The first contains an investigation of the difference between scalp and cortical potentials along with validation of the numerical procedure for cortical current estimation using the back-projected SL.

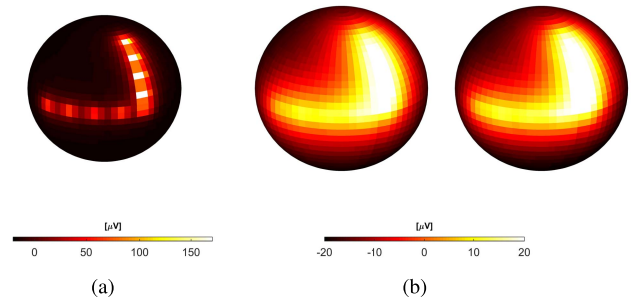


Fig. 4. Forward solution validation. (a) shows the cortical potentials due to the L-shape source distribution. (b) represents the analytical (left) and Sim4Life (right) solutions on the scalp surface.

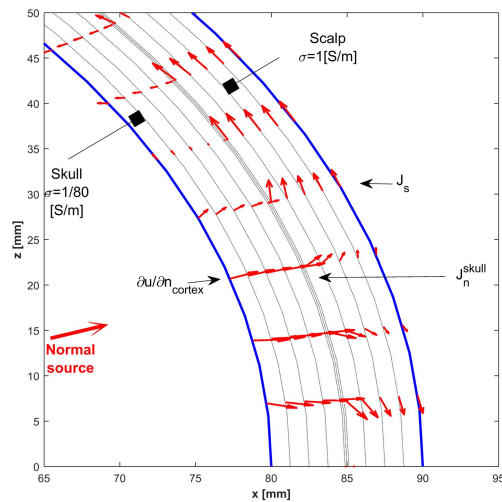


Fig. 5. Current distribution and components involved in the back-projection procedure. XZ plane zoomed view. Inner and outer boundaries are the cortex and scalp surfaces, respectively. Normal dipole location and orientation are schematically drawn with red arrows.

In the second part, results for the BP-CPI algorithm on a spherical head model are presented. The BP-CPI results are compared with the analytical solution for validation. The third part of this section concludes with the BP-CPI performance over a realistic head model. Two real-life source distributions were simulated and comparison between the “true” cortical potentials and the BP-CPI estimation is made with the MN method. The fourth part includes a probabilistic validation of the BP-CPI by a Monte Carlo simulation.

A. Cortical Potentials and Numerical Surface Laplacian

Correct normal cortical current estimation using the *BP-SL* is an important assumption we made when formulating the BP-CPI solution. The correctness of this assumption was tested by comparing the “true” cortical currents to the estimated ones. This was done for the spherical head model, where an analytical solution exists, and for a realistic head model, where only numerical simulations are available for validation. Further investigation was done for two types of brain dipole sources oriented normally and tangentially to the cortex surface, and located 10 mm beneath the cortical surface. A scheme of the test components is shown in Fig. 5. The scheme shows a

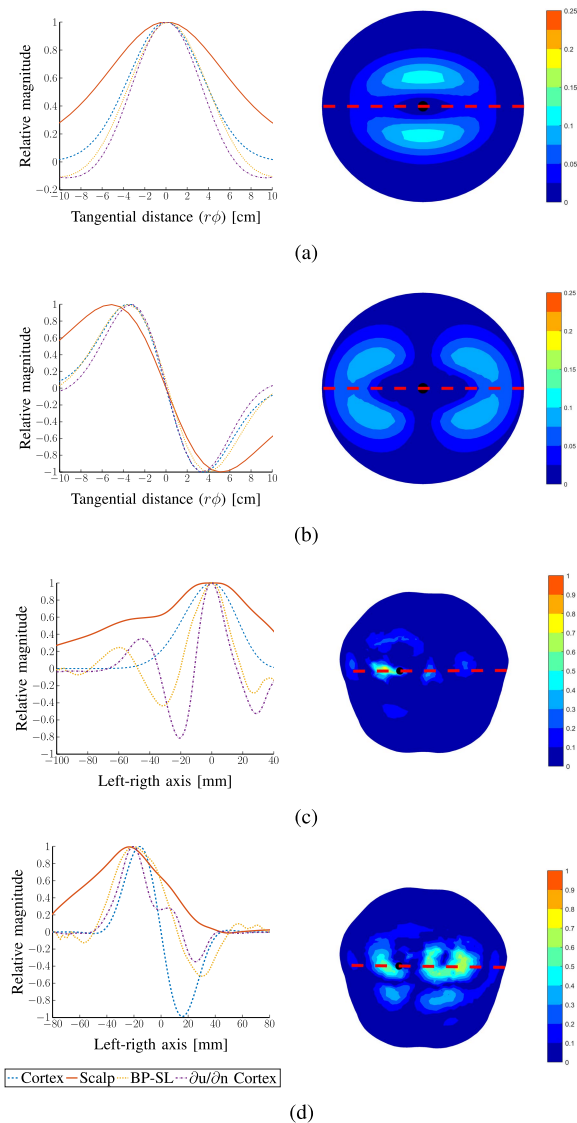


Fig. 6. Validation of the Surface Laplacian as cortical estimator. Each variable was normalized with respect to its peak value. (a) and (b) - results on spherical head model. (c) and (d) results on a realistic head model. (a) and (c) correspond for a normally oriented source, and (b) and (d) for tangentially oriented sources. Right column gives the spatial absolute error between BP-SL and the $\partial u/\partial n_{cortex}$ on a scale between 0 to 1. The left column shows graphs of normalized magnitude for each variable over the dashed red line of the right column. All graphs were aligned so that the origin is at the peak cortical potential point, marked as a black dot in the plots on the right column. Right column scales are quantized to 10 levels for error evaluation.

normally oriented dipole source and the spreading of the scalp currents J_s when reaching the outer surface of the scalp. This effect is used in the SL calculation as depicted in Eq. (6) and (8).

The SL was calculated over the scalp potentials to find an estimation of the skull normal currents J_n^{skull} . This estimated SL is then back-projected onto the cortex surface to find the BP-SL to be used as cortical normal potential derivative $\partial u/\partial n_{cortex}$.

The BP-SL validation results are shown in Fig. 6. Each plot shows the relevant comparison quantities, i.e., cortex potential, scalp potentials, BP-SL, and the “true” normal

oriented electric field ($\partial u/\partial n$) calculated numerically using the two-point symmetric derivative of the “true” potential distribution evaluated by the Sim4Life software for a realistic head model and by the analytical solution for the spherical head model. All quantities’ amplitudes were normalized to better understand the spatial patterns. Figs. 6(a) and 6(b) show the examination results for normally and tangentially oriented sources in a spherical head model, respectively. Figs. 6(c) and 6(d) show the same for a realistic head model. In the spherical head model, the X-axis was selected to be the tangential distance $r\phi$ from the source location, where the source is located at the origin. The tangential distance is used to measure the distance along the sphere surface arc, in [cm]. That is, $r\phi = 0$ is exactly above the source (i.e., the origin), and ϕ changes from $-\pi/2$ to $\pi/2$ along the sphere arc, with r as the sphere radius (80, 85, and 90 mm for cortex, skull, and scalp spheres). For realistic head model plots, the X-axis was selected to be the head left-right axis. One can observe that a high correlation (CC=0.98 and CC=0.99 for normally and tangentially oriented sources, respectively,) of the BP-SL to the analytic solution is obtained for a spherical head model and a satisfying correlation (CC=0.86 and CC=0.75 for normally and tangentially oriented source, respectively) for the realistic head model. The BP-SL diversion from the actual cortical currents can be related to a non-perfect scalp-cortex projection that contains errors in some regions of the head. This can be viewed in Fig. 6(c), where the BP-SL on the positive axis is a very good estimation of the cortical currents, whereas in the negative region, the BP-SL follows the cortical currents with about 15 mm offset. It is hard to compensate for these kinds of effects in all scalp signals.

B. BP-CPI on Spherical Head Model

As the first step in the validation of the BP-CPI algorithm, it was applied on the spherical scalp potential distribution. The source distribution (positive sources) shown in Fig. 7(a) is similar to the one used in the validation of the forward solution described in section II-E, but with sources positioned 10 mm underneath the cortex surface, instead of 5 mm as shown in Fig. 4, and oriented normal to the cortex in the negative direction (i.e., inward). The analytical solutions of the scalp and cortex potentials distribution are shown in Figs. 7(b) and 7(c), respectively. The estimated cortical potential distribution using BP-CPI can be viewed in Fig. 7(d). By visual inspection, one can observe that the algorithm results are in very good agreement with the cortical potential, resulting in a very high CC, and very low RE, between the analytical and estimated cortical potentials (CC=0.997, RE=0.0078).

C. Illustration of BP-CPI on Realistic Head Model for Practical Cases

The BP-CPI is a robust technique for estimation of the cortical potentials by only holding the knowledge of scalp electrodes and head model information, acquired from a single subject or averaged MRI T1 scan. This section shows the BP-CPI algorithm accuracy for two typical simulated sources

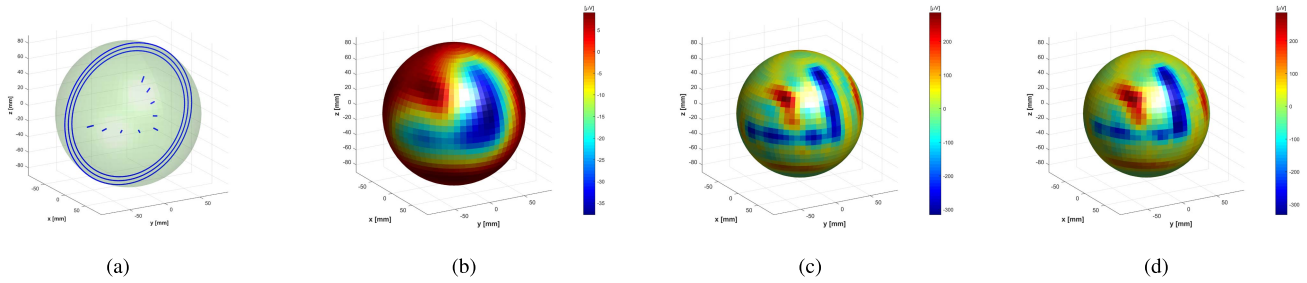


Fig. 7. BP-CPI validation on spherical head model. (a) Sources' orientation and location used for validation. Blue circles illustrate the boundaries of the scalp, skull, and cortex spheres. (b) and (c) are the analytical forward solutions on the scalp and cortical surfaces, respectively. (d) The estimated cortical potentials using the scalp potentials with the BP-CPI algorithm.

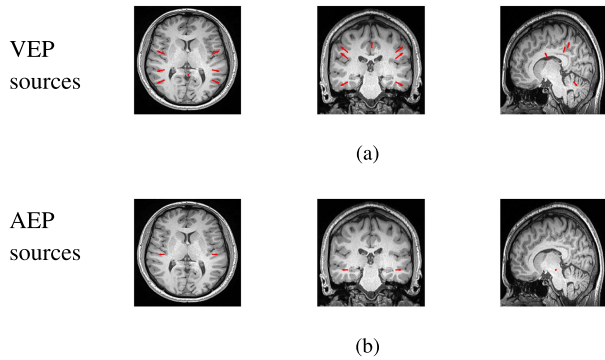


Fig. 8. Source distributions for BP-CPI validation on a realistic head model. From left to right: axial, coronal, and sagittal views of the subject MRI, incorporating seven VEP (a) and two AEP (b) source locations and orientations

that are based on the brain activity excited by auditory and visual stimuli, denoted here as auditory evoked potentials (AEP) and visually evoked potentials (VEP). Both sources' distributions are based on well-established source locations given in relevant literature [44], [45] and shown in Fig. 8. Forward solution was obtained for each of the selected VEP and AEP source distributions. Results are shown in Fig. 9. Scalp potentials were sampled at 124 sites according to EGI128 electrodes system, and the BP-CPI algorithm was used to generate estimated cortical potentials. The BP-CPI results are also shown in Figs. 9(c) and 9(g) for VEP and AEP source distributions, respectively. It is noted that these source locations and orientations are only used for the BP-CPI validation process and not for the validation of measured auditory or visual stimuli-based EEG data.

In order to compare the BP-CPI to other CPI methods, we implemented the minimum-norm (MN) estimation method [14]. The MN estimates the three-dimensional brain source distribution with the smallest two-norm solution vector that would match the measured EEG data. This method (and its' variations) is well-known and was used in many applications [13], [46]–[49] to enhance the spatial resolution acquired using EEG. The MN method results are seen in Figs. 9(d) and 9(h) for the VEP and AEP, respectively.

In the case of VEP sources, it is clearly seen that the two sources at the inferior fronto-parietal cortex were estimated with very high similarity to the “true” cortical potentials by

the BP-CPI. The single source at the lateral inferior temporal cortex was localized, but with lower amplitude, due to the effect of large skull thickness and non-optimal SL projection factor in that region. The same inferences can be deduced while inspecting the results for the AEP. The BP-CPI localizes the cortical sources at the superior temporal lobe area with very good agreement with the “true” cortical potentials.

Table II shows a quantitative measure of the agreement between the estimated and “true” cortical potentials. Measures were calculated for both BP-CPI and MN methods, for both AEP and VEP cases. The CC and RE were calculated for the whole cortical surface and for the region of interest (ROI), which contains the most energy in each case and is marked with a black dashed line in Figs. 9(c) and 9(g). It can be seen that the results of the BP-CPI gives an accurate solution in regions where the signal is high, which are mostly the regions of high clinical interest, and a fine estimation for the whole cortical surface. When quantitatively comparing the BP-CPI and the MN methods, one can also observe that there is a good estimation for the AEP. However, for the VEP case, the BP-CPI gives a much better approximation than the MN.

D. Probabilistic Validation

To better approximate the BP-CPI performance for the general case, our simulations included a large random sampling of source locations to provide an average estimate of BP-CPI accuracy. This was done by a Monte Carlo simulation. Either one, two, or three sources were randomly located within the cortical volume. Sources' orientations were also defined normally to the cortical surface. The random selection ensures no systematic region-activation bias in these model studies. One a priori constraint on the locations of the sources was taken - all sources were located at a distance no larger than 40 mm from the cortical surface. This constraint was taken to simulate pure cortical sources, which are the main target of estimation for the BP-CPI. All simulations were performed with the same realistic head model presented in Sec. II-C. In order to eliminate any tendency to each of the source configuration types, we randomly selected 400 distributions for each type of source configuration as shown in Table III. In total, 1200 source configurations were used as a part of the probabilistic validation stage.

Sim4Life was used to simulate the “true” cortical and scalp potentials due to each of the source configurations.

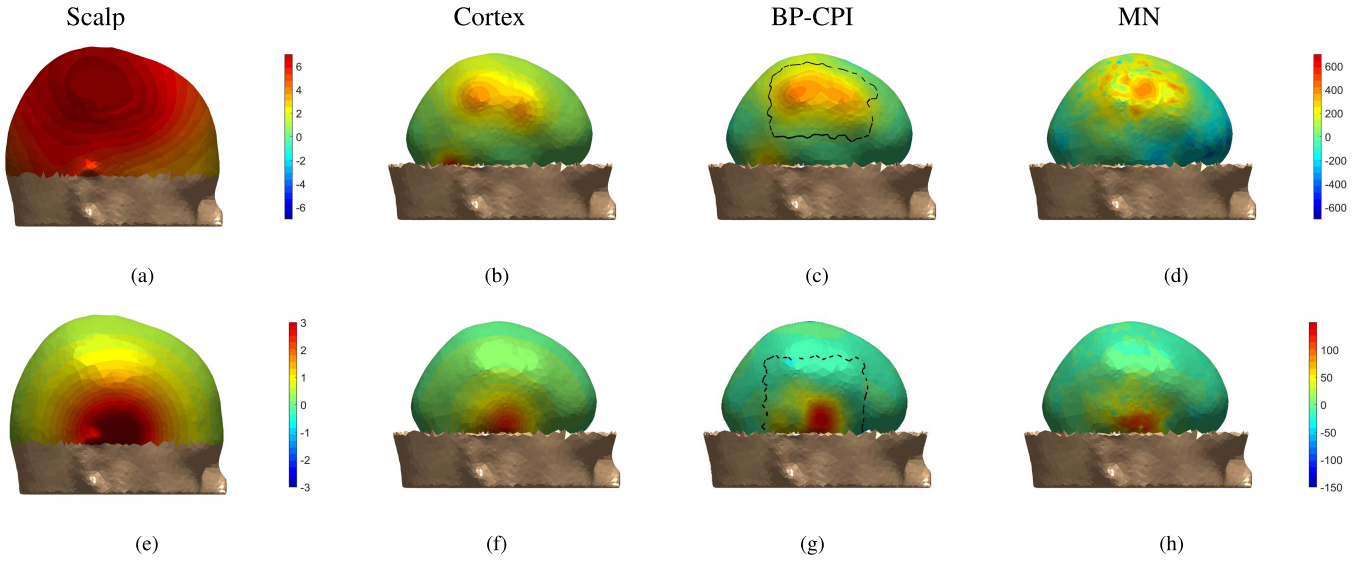


Fig. 9. BP-CPI results on realistic head model. (a)-(d) are results for the VEP case. (e)-(h) are results for the AEP case. From left to right: scalp reference potentials (forward solution), cortex reference potentials, BP-CPI estimation, and MN estimation. All scales are in $[\mu V]$ units. Cortex reference signal, BP-CPI, and MN estimations share the same scale. ROIs are marked over (c) and (g).

TABLE II

CORRELATION BETWEEN “TRUE” AND ESTIMATED CORTICAL POTENTIALS FOR THE BP-CPI AND MN METHODS

| Model | CC | RE | CC (ROI) | RE(ROI) |
|----------------|------|------|----------|---------|
| VEP_{BP-CPI} | 0.78 | 0.1 | 0.97 | 0.04 |
| AEP_{BP-CPI} | 0.82 | 0.12 | 0.98 | 0.05 |
| VEP_{MN} | 0.52 | 0.21 | 0.39 | 0.88 |
| AEP_{MN} | 0.8 | 0.07 | 0.98 | 0.02 |

TABLE III

MONTE CARLO SIMULATION RESULTS

| Source distribution | Count | Mean | SD |
|---------------------|-------|------|------|
| Single source | 400 | 0.78 | 0.11 |
| Two sources | 400 | 0.84 | 0.04 |
| Three sources | 400 | 0.84 | 0.05 |
| All sources | 1200 | 0.82 | 0.11 |

Then, the scalp potentials were sampled at the electrodes’ locations and the BP-CPI was used to estimate the cortical potential. Finally, CC measure was calculated between the “true” and estimated cortical potentials. In these model studies, the EEG system was selected to be the EGI128, as presented in Sec. II-C. Fig. 10 shows the results of the Monte Carlo study with a histogram representation. The results show a relatively normal distribution with negative skewness. Numerical values for the mean and standard deviation (SD) are given in Table III.

E. Noise Sensitivity

The effect of electrodes noise on the BP-CPI estimation was also investigated. Additive white Gaussian noise (AWGN) was added to the noise-free scalp electrodes potentials to form

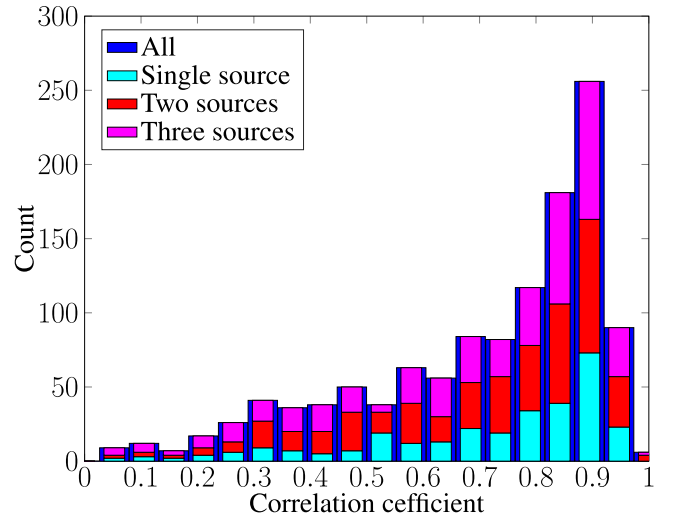


Fig. 10. Histogram presentation of the Monte Carlo simulation results.

the noisy electrodes potentials, measured by the EGI128 electrodes system. These noisy electrodes potentials were used to estimate the cortical potentials using the BP-CPI and the MN methods. Our tests include two common EEG levels of AWGN noise with SD defined by (20), where $n_{level} = 0.05, 0.1$ for 5% or 10% noise levels, respectively.

$$SD_n = \max\{u_{scalp}\} \cdot n_{level} \quad (20)$$

Noise was added to EEG potentials excited by the VEP and AEP source distributions, and the same noise vector was used to test both cases with both CPI methods. Results are shown in Fig. 11. BP-CPI and MN estimation results are shown for the AEP and VEP cases for two levels of noise. In addition, the “true” cortical potentials are given for reference. The noisy electrodes introduce spatial artifacts to the BP-CPI estimation, even though the main activation still remains clear for both

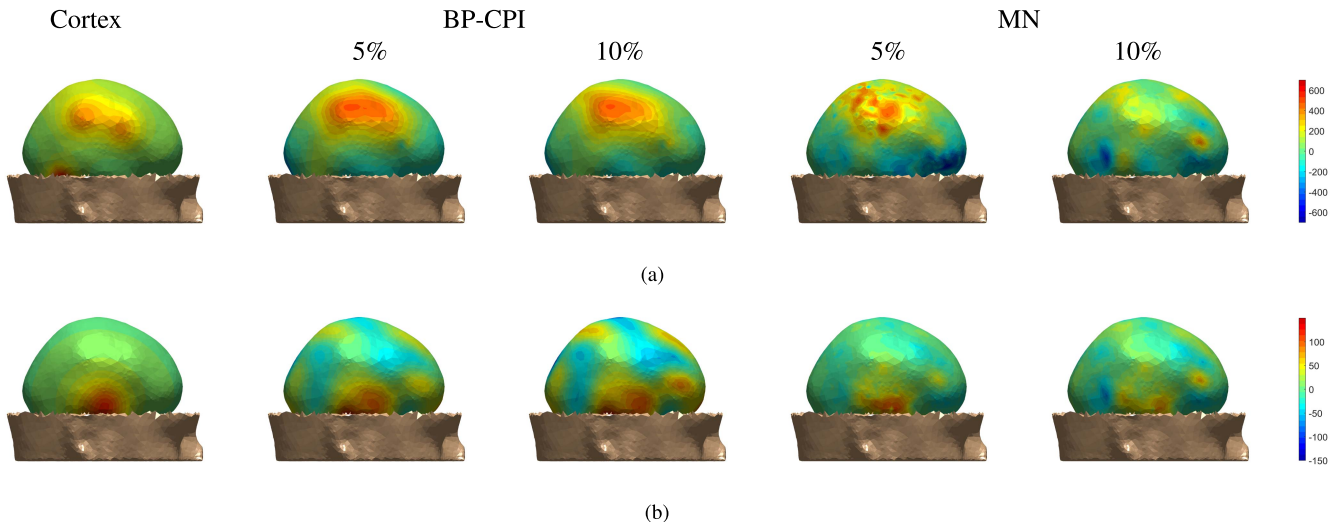


Fig. 11. BP-CPI sensitivity to noise. From left to right: “true” cortical potentials, BP-CPI results for 5% and 10% noise, MN results for 5% and 10% noise. (a) and (b) correspond to the VEP and AEP cases, respectively. All results for each case share the same scale and the units are [μV].

noise levels; this is mostly seen in the case of the AEP, where spatial artifacts are seen and their amplitude increases with the noise level. This observation can be seen in BP-CPI solutions to the VEP and AEP cases, and their strength is directly proportional to n_{level} . When examining the MN results, we see that the noise did not alter the spatial pattern of the cortical potentials at the ROI, but considerably changed its total energy.

In order to quantitatively compare the estimated and “true” cortical potentials, CC and RE were averaged over 10 tests; quantitative results are given in Table IV. It is seen that higher noise level decreases the CC and increases the RE for both CPI methods. The artifacts shown in BP-CPI results of Fig. 11 lower the CC by less than 0.3 (RE is less than 0.12), for the 5% noise level, and by less than 0.42 (RE is less than 0.23) for the 10% noise level. When observing the ROI, the CC decreases by less than 0.1, and the RE by less than 0.04, for the worst case of the 10% noise level. In comparison to the BP-CPI, the MN method gives less accurate results and gives a decrease of less than 0.08 in CC and less than 0.15 in RE, for the 5% noise level. For the higher noise level, the MN drops to a decrease of less than 0.27 in CC and less than 0.46 in RE. These results suggest that the BP-CPI can give a good estimation of the cortical potentials, even in the presence of common EEG noise levels.

IV. DISCUSSION

A new method for the estimation of cortical potentials using a realistic head model was proposed and presented. The new method uses FEM solver and estimates the cortical potential normal derivative in order to find an accurate solution to the cortical potentials. The algorithm uses only sampled scalp potentials with the realistic head model physical geometry and its conductivity values, to produce a cortical potentials estimation that is the product of both the normal and tangential currents flowing from within the brain. The method solves the LE using two BCs wrapping the entire solution volume. This technique modifies the problem from a classic ill-posed inverse-problem to a forward-problem variation having

TABLE IV
SENSITIVITY TO NOISE FOR THE BP-CPI AND MN METHODS.
MEASURES ARE (CC/RE)

| Sources | Region | noise (5%) | noise (10%) |
|----------------|------------|---------------|---------------|
| VEP_{BP-CPI} | All cortex | (0.68 / 0.22) | (0.61 / 0.26) |
| | ROI | (0.95 / 0.05) | (0.9 / 0.07) |
| AEP_{BP-CPI} | All cortex | (0.53 / 0.22) | (0.4 / 0.35) |
| | ROI | (0.92 / 0.07) | (0.88 / 0.08) |
| VEP_{MN} | All cortex | (0.49 / 0.36) | (0.25 / 0.67) |
| | ROI | (0.36 / 0.9) | (0.17 / 1.12) |
| AEP_{MN} | All cortex | (0.74 / 0.17) | (0.54 / 0.3) |
| | ROI | (0.84 / 0.04) | (0.67 / 0.1) |

advantages such as uniqueness and stability of the solution. The implementation of the method is straightforward and utilizes only standard linear algebra computation, which was programmed on an ordinary laptop computer with fast calculation time of only a few seconds. Three validation stages were performed in order to examine the algorithm performance, which was shown to be very good on both spherical and realistic head models. The first validation stage tested the validity of the back-projected SL, which was found to be a very good cortical current estimator for both spherical and realistic head models. The second and third validation stages tested the whole BP-CPI algorithm, initially on a spherical head model and then on a realistic head model. Both steps gave very good results with CC of 0.99 for spherical model, and above 0.97 for a realistic model within the region of interest.

We continued with the validation stage in two directions: The first, in order to eliminate the chance that the above results were not obtained by chance, we conducted a Monte Carlo simulation, including 1200 source configurations and found that the BP-CPI gives good results (mean CC of 0.82) for the general case. It can also be deduced that when the number of dominant sources is no larger than 3, the

BP-CPI gives relatively the same accuracy for all three types of source configuration. We do expect a decrease in the accuracy for more simultaneous sources. These results show that the BP-CPI gives an estimation that is robust through most types of cortical potentials. The second direction we took for validating the BP-CPI is comparison versus another well-known CPI method. The selected method was the MN, which gave relatively good results when dealing with spatially separated sources, such as the investigated AEP sources presented here. When we tested the two methods on a more complicated cortical potential distribution, such as the VEP that is comprised of multiple close sources, the BP-CPI gave better estimation ($CC_{BP-CPI} = 0.78$ versus $CC_{MN} = 0.52$). We believe that this is caused by the inherent constraint of the MN to find the solution with the minimum energy. Thus, in the case of multiple close sources, the solution with the minimum energy that has the most similar forward solution to the measured EEG scalp potentials will be many scattered cortical activations, as seen in the results in Fig. 9(d).

Further investigation of the BP-CPI performance was done by examination of the effect of noise on the estimation quality. Two typical noise levels (5% and 10%) were added to the scalp potentials and the BP-CPI and MN methods were applied on these noisy potentials to estimate the cortical potentials. The BP-CPI showed low susceptibility to the added noise, as was the MN. The MN method seems to generate fewer spatial artifacts, but the main activations strength is weakened for higher noise levels. This is due to the regularization term in the MN solution that increases the solution robustness to noise, but lowers the energy of the overall cortical potentials. On the other hand, the BP-CPI keeps the strength of the highest activation with high accuracy, but adds spurious spatial artifacts that increase with noise level that is linearly connected to their amplitude.

Based on these results, and the fact that very powerful research tools were developed to generate them, we find it important to further investigate the BP-CPI method properties and performance. This brought us to initiate a fifth validation stage of sensitivity analysis for the proposed method, examining the effect of scalp electrodes number, noise, and displacement error. In addition, the sensitivity analysis will assess the influence of tissue conductivity estimation errors and the impact of different source numbers, locations, and orientations on the cortical potential estimations. This future BP-CPI validation will also include *in vivo* experimental validation, which involves analysis of simultaneous measurements of fMRI and EEG during the performance of a cognitive task. In order to have full understanding of the BP-CPI in *in vivo* situation, this experiment is carried out with no less than 30 subjects.

BP-CPI gives a simple, fast, non-parametric, and very accurate high resolution estimation for the cortical potentials on a realistic head model of a single subject. The novelty of this paper is threefold. For the first time to the authors' knowledge, the numerical estimation of the scalp surface Laplacian is back-projected onto the cortex to serve as boundary conditions of the cortical normal currents. Second, the BP-CPI method solves the LE with boundary conditions

wrapping the whole solution volume to generate a single, unique, and non-parametric solution; and third, our detailed realistic head model accounts for the diploe spongy bone and air cavities as separate layers inside the head volume, which, with our in-house developed FEM solver, gives an even more realistic model to use in the BP-CPI solution.

With the BP-CPI, researchers have the opportunity to acquire accurate estimations for cortical potentials of ongoing or event-related potentials, sampled at the scalp of a massive number of subjects in order to have better neurological inferences from very detailed cortical potentials' spatio-temporal patterns. This can be accomplished by integrating the BP-CPI algorithm into more powerful monitoring tools that will make use of the cortical potentials' variations in space and time, such as brain network activation (BNA) [50] or STEP algorithm [51]. High level analysis combined with more focused cortical potential maps can reveal brain functionality information that was not yet available to the clinician.

Once all validation stages are finished, and the method results found to be satisfactory, we aim at integrating the BP-CPI into monitoring and stimulation tools. The integration of the BP-CPI with neuro-modulation tools such as transcranial magnetic stimulation (TMS), deep TMS (dTMS), and transcranial electrical stimulation, can provide improved clinical assessment and treatment. Clinical assessment improvement can be achieved by applying the BP-CPI to EEG signals acquired during therapeutic procedures and maintaining high resolution cortical potentials for better understanding the effect of these procedures on the subjects' cortex. Shahar *et al.* in [52], used scalp EEG to find an objective diagnostic tool for the assessment of attention-deficit-hyperactivity-disorder (ADHD) severity during dTMS treatment. Combining the BP-CPI with this type of neuro-modulation tool will provide a better focal monitoring tool for such applications. Treatment improvement can be accomplished by applying the BP-CPI during therapeutic procedures. Improved localization of the stimulation peak power will help clinicians improve therapy and avoid subjects pain and side effects caused by activation of undesired cortical areas, and maintain real-time monitoring of the activated cortical areas during the treatment. Tools such as Brainsight TMS navigation (Rogue Resolutions Ltd.) indicate the recommended location for the TMS coil in order to target a specific cortical location only by means of coil location and orientation around the subjects' scalp. However, this tool (and others) can't provide monitoring of the treatment-targeted cortical area. Applying the BP-CPI to the EEG signal acquired exactly at the moment of the peak current of the TMS coil will give online estimation of the cortical activation as a result of the TMS. BP-CPI can provide a good monitoring tool for the treatment effects, enable improved therapy, and provide means to close the treatment loop in the future.

ACKNOWLEDGMENTS

The authors would like to thank Efrat Sasson (Wise-Image) for her contribution to the realistic head modeling.

REFERENCES

- [1] P. L. Nunez and R. Srinivasan, *Electric Fields Brain: Neurophysics EEG*. London, U.K.: Oxford Univ. Press, 2006.
- [2] F. Perrin, O. Bertrand, and J. Pernier, "Scalp current density mapping: Value and estimation from potential data," *IEEE Trans. Biomed. Eng.*, vol. BME-34, no. 4, pp. 283–288, Apr. 1987.
- [3] F. Babiloni, C. Babiloni, F. Carducci, M. Del Gaudio, P. Onorati, and A. Urbano, "A high resolution EEG method based on the correction of the surface Laplacian estimate for the subject's variable scalp thickness," *Electroencephalogr. Clin. Neurophysiol.*, vol. 103, no. 4, pp. 486–492, 1997.
- [4] D. L. Schomer and F. L. Da Silva, *Niedermeyer's Electroencephalography: Basic Principles, Clinical Applications, and Related Fields*. Baltimore, MD, USA: Williams & Wilkins, 2012.
- [5] B. He, "Brain electric source imaging: Scalp laplacian mapping and cortical imaging," *Critical Rev. Biomed. Eng.*, vol. 27, nos. 3–5, pp. 149–188, 1998.
- [6] C. M. Michel, M. M. Murray, G. Lantz, S. Gonzalez, L. Spinelli, and R. G. de Peralta, "EEG source imaging," *Clin. Neurophysiol.*, vol. 115, no. 10, pp. 2195–2222, Oct. 2004.
- [7] P. C. Hansen, "Truncated singular value decomposition solutions to discrete ill-posed problems with ill-determined numerical rank," *SIAM J. Sci. Statist. Comput.*, vol. 11, no. 3, pp. 503–518, 1990.
- [8] S. Iwaki and S. Ueno, "Weighted minimum-norm source estimation of magnetoencephalography utilizing the temporal information of the measured data," *J. Appl. Phys.*, vol. 83, no. 11, pp. 6441–6443, 1998.
- [9] R. D. Pascual-Marqui, C. M. Michel, and D. Lehmann, "Low resolution electromagnetic tomography: A new method for localizing electrical activity in the brain," *Int. J. Psychophysiol.*, vol. 18, no. 1, pp. 49–65, Oct. 1994.
- [10] K. Miller, "Least squares methods for ill-posed problems with a prescribed bound," *SIAM J. Math. Anal.*, vol. 1, no. 1, pp. 52–74, 1970.
- [11] R. G. de Peralta Menendez, M. M. Murray, C. M. Michel, R. Martuzzi, and S. L. G. Andino, "Electrical neuroimaging based on biophysical constraints," *NeuroImage*, vol. 21, no. 2, pp. 527–539, Feb. 2004.
- [12] Y. Lai *et al.*, "Noninvasive cortical imaging of epileptiform activities from interictal spikes in pediatric patients," *NeuroImage*, vol. 54, no. 1, pp. 244–252, Jan. 2011.
- [13] Y. Kanamori *et al.*, "Minimum norm estimates in MEG can delineate the onset of interictal epileptic discharges: A comparison with ECoG findings," *NeuroImage, Clin.*, vol. 2, pp. 663–669, Apr. 2013.
- [14] M. S. Hämäläinen and R. J. Ilmoniemi, "Interpreting magnetic fields of the brain: Minimum norm estimates," *Med. Biol. Eng. Comput.*, vol. 32, no. 1, pp. 35–42, Jan. 1994.
- [15] B. He, X. Zhang, J. Lian, H. Sasaki, D. Wu, and V. L. Towle, "Boundary element method-based cortical potential imaging of somatosensory evoked potentials using subjects' magnetic resonance images," *NeuroImage*, vol. 16, no. 3, pp. 564–576, Jul. 2002.
- [16] Y. Lu, L. Yang, G. A. Worrell, B. Brinkmann, C. Nelson, and B. He, "Dynamic imaging of seizure activity in pediatric epilepsy patients," *Clin. Neurophysiol.*, vol. 123, no. 11, pp. 2122–2129, Nov. 2012.
- [17] B. He, Y. Wang, and D. Wu, "Estimating cortical potentials from scalp EEGs in a realistically shaped inhomogeneous head model by means of the boundary element method," *IEEE Trans. Biomed. Eng.*, vol. 46, no. 10, pp. 1264–1268, Oct. 1999.
- [18] P. R. Johnston and R. M. Gulrajani, "Selecting the corner in the L-curve approach to Tikhonov regularization," *IEEE Trans. Biomed. Eng.*, vol. 47, no. 9, pp. 1293–1296, Sep. 2000.
- [19] P. C. Hansen, "Rank-deficient and discrete ill-posed problems: Numerical aspects of linear inversion," *Soc. Ind. Appl. Math.*, 1998.
- [20] C. R. Vogel, *Computational Methods for Inverse Problems*, vol. 23. Philadelphia, PA, USA: SIAM, 2002.
- [21] J. Le and A. Gevins, "Method to reduce blur distortion from EEG's using a realistic head model," *IEEE Trans. Biomed. Eng.*, vol. 40, no. 6, pp. 517–528, Jun. 1993.
- [22] P. Valdes-Sosa, F. Marti, F. Garcia, and R. Casanova, "Variable resolution electric-magnetic tomography," in *Biomag 96*, C.J. Aine, G. Stroink, C. C. Wood, Y. Okada, and S. J. Swithenby, Eds. New York, NY, USA: Springer, 2000, pp. 373–376.
- [23] D. McNay, E. Michielssen, R. L. Roger, S. A. Taylor, M. Akhtari, and W. W. Sutherling, "Multiple source localization using genetic algorithms," *J. Neurosci. Methods*, vol. 64, no. 2, pp. 163–172, Feb. 1996.
- [24] Y. Yamashita, "Theoretical studies on the inverse problem in electrocardiography and the uniqueness of the solution," *IEEE Trans. Biomed. Eng.*, vol. BME-29, no. 11, pp. 719–725, Nov. 1982.
- [25] L. Soufflet, M. Toussaint, R. Luthringer, J. Gresser, R. Minot, and J. P. Macher, "A statistical evaluation of the main interpolation methods applied to 3-dimensional EEG mapping," *Electroencephalogr. Clin. Neurophysiol.*, vol. 79, no. 5, pp. 393–402, Nov. 1991.
- [26] J. Le, V. Menon, and A. Gevins, "Local estimate of surface Laplacian derivation on a realistically shaped scalp surface and its performance on noisy data," *Electroencephalogr. Clin. Neurophysiol./Evoked Potentials Section*, vol. 92, no. 5, pp. 433–441, Sep. 1994.
- [27] M. Okamoto and I. Dan, "Automated cortical projection of head-surface locations for transcranial functional brain mapping," *NeuroImage*, vol. 26, no. 1, pp. 18–28, May 2005.
- [28] P. L. Nunez, R. B. Silberstein, P. J. Cadusch, R. S. Wijesinghe, A. F. Westdorp, and R. Srinivasan, "A theoretical and experimental study of high resolution EEG based on surface Laplacians and cortical imaging," *Electroencephalogr. Clin. Neurophysiol.*, vol. 90, no. 1, pp. 40–57, Jan. 1994.
- [29] R. V. Uitert, C. Johnson, and L. Zhukov, "Influence of head tissue conductivity in forward and inverse magnetoencephalographic Simulations using realistic head models," *IEEE Trans. Biomed. Eng.*, vol. 51, no. 12, pp. 2129–2137, Dec. 2004.
- [30] J. Ashburner and K. J. Friston, "Unified segmentation," *NeuroImage*, vol. 26, no. 3, pp. 839–851, 2005.
- [31] S. M. Smith, "Fast robust automated brain extraction," *Human Brain Mapping*, vol. 17, no. 3, pp. 143–155, 2002.
- [32] Q. Fang and D. A. Boas, "Tetrahedral mesh generation from volumetric binary and grayscale images," in *Proc. IEEE Int. Symp. Biomed. Imag., Nano Macro (ISBI)*, Jun. 2009, pp. 1142–1145.
- [33] V. Montes-Restrepo, P. van Mierlo, G. Strobbe, S. Staelens, S. Vandenberghe, and H. Hallez, "Influence of skull modeling approaches on EEG source localization," *Brain Topogr.*, vol. 27, no. 1, pp. 95–111, Jan. 2014.
- [34] M. Dannhauer, B. Lanfer, C. H. Wolters, and T. R. Knösche, "Modeling of the human skull in EEG source analysis," *Human Brain Mapping*, vol. 32, no. 9, pp. 1383–1399, Sep. 2011.
- [35] C. Ramon, P. Garguilo, E. A. Fridgerisson, and J. Hauelsen, "Changes in scalp potentials and spatial smoothing effects of inclusion of dura layer in human head models for EEG simulations," *Frontiers Neuroeng.*, vol. 7, p. 32, Aug. 2014, doi: 10.3389/fneng.2014.00032.
- [36] M. Fuchs, M. Wagner, and J. Kastner, "Development of volume conductor and source models to localize epileptic foci," *J. Clin. Neurophysiol.*, vol. 24, no. 2, pp. 101–119, 2007.
- [37] V. Fonov, A. C. Evans, K. Botteron, C. R. Almli, R. C. McKinstry, and D. L. Collins, "Unbiased average age-appropriate atlases for pediatric studies," *NeuroImage*, vol. 47, no. 1, pp. 313–327, 2009.
- [38] M. W. Slutzky, L. R. Jordan, T. Krieg, M. Chen, D. J. Mogul, and L. E. Miller, "Optimal spacing of surface electrode arrays for brain-machine interface applications," *J. Neural Eng.*, vol. 7, no. 2, p. 026004, 2010.
- [39] J. L. Volakis, A. Chatterjee, and L. C. Kempel, *Finite Element Method Electromagnetics: Antennas, Microwave Circuits, and Scattering Applications*, vol. 6. Hoboken, NJ, USA: Wiley, 1998.
- [40] J. Webb, "Imposing linear constraints in finite-element analysis," *Commun. Appl. Numer. Methods*, vol. 6, no. 6, pp. 471–475, Aug. 1990.
- [41] Z. Z. M. Ag and C. Zürich, "Sim4life: A simulation platform for life sciences and medtech applications," *Eur. Cells Mater.*, vol. 27, no. 2, p. 6, 2014.
- [42] G. Rizzolatti and G. Luppino, "The cortical motor system," *Neuron*, vol. 31, no. 6, pp. 889–901, Sep. 2001.
- [43] N. Boddart *et al.*, "Perception of complex sounds in autism: Abnormal auditory cortical processing in children," *Amer. J. Psychiatry*, vol. 161, no. 11, pp. 2117–2120, Nov. 2004.
- [44] F. Di Russo, A. Martínez, M. I. Sereno, S. Pitzalis, and S. A. Hillyard, "Cortical sources of the early components of the visual evoked potential," *Human Brain Mapping*, vol. 15, no. 2, pp. 95–111, Feb. 2002.
- [45] M. Huotilainen *et al.*, "Combined mapping of human auditory EEG and MEG responses," *Electroencephalogr. Clinical Neurophysiology/Evoked Potentials Section*, vol. 108, no. 4, pp. 370–379, 1998.
- [46] O. Hauk, "Keep it simple: A case for using classical minimum norm estimation in the analysis of EEG and MEG data," *NeuroImage*, vol. 21, no. 4, pp. 1612–1621, Apr. 2004.

- [47] H. Yuan, A. Doud, A. Gururajan, and B. He, "Cortical imaging of event-related (de)synchronization during online control of brain-computer interface using minimum-norm estimates in frequency domain," *IEEE Trans. Neural Syst. Rehabil. Eng.*, vol. 16, no. 5, pp. 425–431, Oct. 2008.
- [48] X. Bai, V. L. Towle, E. J. He, and B. He, "Evaluation of cortical current density imaging methods using intracranial electrocorticograms and functional MRI," *NeuroImage*, vol. 35, no. 2, pp. 598–608, Apr. 2007.
- [49] G. Lantz, R. G. de Peralta, L. Spinelli, M. Seeck, and C. M. Michel, "Epileptic source localization with high density EEG: How many electrodes are needed?" *Clin. Neurophysiol.*, vol. 114, no. 1, pp. 63–69, Jan. 2003.
- [50] G. Shahaf *et al.*, "Introducing a novel approach of network oriented analysis of ERPs, demonstrated on adult attention deficit hyperactivity disorder," *Clin. Neurophysiol.*, vol. 123, no. 8, pp. 1568–1580, Aug. 2012.
- [51] Y. Stern, A. Reches, and A. B. Geva, "Brain network activation analysis utilizing spatiotemporal features for event related potentials classification," *Frontiers Comput. Neurosci.*, vol. 10, pp. 1–11, Dec. 2016.
- [52] H. Shahar *et al.*, "Right prefrontal deep TMS effects on attention symptoms: Behavioral outcomes and electrophysiological correlates," *Eur. Psychiatry*, vol. 30, p. 841, 2015.